LANGMUIR

pubs.acs.org/Langmuir Article

Nonlinear Transient and Steady State Stretching of Deflated Vesicles in Flow

Dinesh Kumar and Charles M. Schroeder*

Cite This: *Langmuir* 2021, 37, 13976−13984 Read Online

ACCESS | Metrics & More | Article Recommendations | Supporting Information

ABSTRACT: Membrane-bound vesicles and organelles exhibit a wide array of nonspherical shapes at equilibrium, including biconcave and tubular morphologies. Despite recent progress, the stretching dynamics of deflated vesicles is not fully understood, particularly far from equilibrium where complex nonspherical shapes undergo large deformations in flow. Here, we directly observe the transient and steady-state nonlinear stretching dynamics of deflated vesicles in extensional flow using a Stokes trap. Automated flow control is used to observe vesicle dynamics over a wide range of flow rates, shape anisotropy, and viscosity contrast. Our results show that deflated vesicle membranes stretch into highly deformed shapes in flow above a critical capillary number Ca_{c_1}. We further identify a second critical capillary number Ca_{c_2}, above which vesicle stretch diverges in flow. Vesicles are robust to multiple nonlinear stretch−relax cycles, evidenced by relaxation of dumbbell-shaped vesicles containing thin lipid tethers following flow cessation. An analytical model is developed for vesicle deformation in flow, which enables comparison of nonlinear steady-state stretching results with theories for different reduced volumes. Our results show that the model captures the steady-state stretching of moderately deflated vesicles; however, it underpredicts the steady-state nonlinear stretching of highly deflated vesicles. Overall, these results provide a new understanding of the nonlinear stretching dynamics and membrane mechanics of deflated vesicles in flow.

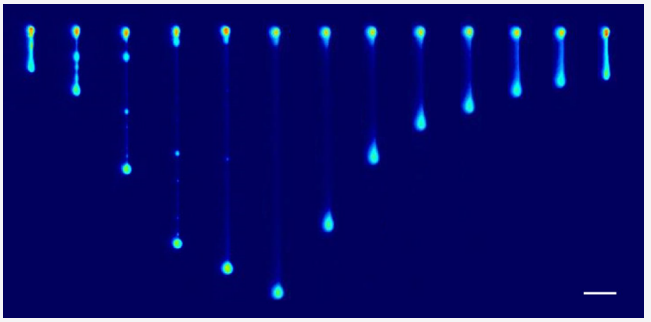

INTRODUCTION

Membrane-bound vesicles and cells with nonspherical shapes are commonly found in biology. Red blood cells (RBCs) exhibit biconcave disc shapes at equilibrium that increase surface area to enhance oxygen transport across the membrane. RBCs also undergo repeated, large-amplitude mechanical deformations while flowing through microvessels.[1−3] From this view, there is a clear need to understand the nonequilibrium dynamics and mechanics of membrane-bound vesicles with tubular or biconcave morphologies, including the role of membrane deformability, which will reveal new insight into the mechanics and transport properties of cells.[4,5] Prior work on vesicle mechanics has largely focused on nearly spherical vesicle morphologies in the weak deformation regime using micropipette aspiration,[6,7] electrodeformation,[8−10] optical trapping,[11−14] and sedimentation.[15,16]

In recent years, vesicle dynamics have been studied in defined hydrodynamic flows including capillary flow,[1,17−19] simple shear,[20−24] pure extension,[25−30] and linear mixed flows.[31,32] Vesicle morphology in flow depends on flow strength and shape anisotropy. The reduced volume ν is a measure of vesicle shape anisotropy, such that $\nu = 1$ corresponds to a perfect sphere. In Poiseuille flow, weakly deflated vesicles ($\nu \geq 0.7$) adopt an axisymmetric parachute shape with a concave terminus or a bullet-like shape with a convex terminus depending on flow strength.[33−36] For highly deflated vesicles ($\nu < 0.7$), a slipper-like shape is observed over a wide range of flow rates.[34] In shear flow, vesicles undergo three different dynamical motions including: (i) tumbling (TU) motion in which the vesicle exhibits full periodic rotations ($\phi = 2\pi$) with respect to the flow-axis, (ii) tank-treading (TT) motion in which an ellipsoidal vesicle's major axis maintains a constant angle with respect to the flow-axis and the membrane rotates around this fixed ellipsoidal shape, and (iii) trembling (TR) motion in which the vesicle's major axis oscillates around the flow-axis but never reaches $\phi = \pi/2$. Classic work by Keller and Skalak[37] for ellipsoidal-shaped vesicles with negligible thermal fluctuations theoretically predicted tumbling and tank-treading dynamics, which was experimentally observed several years later by Kantsler and co-workers in 2006.[22] Theoretical modeling by Misbah and co-workers revealed the trembling behavior of vesicles in shear

Received: May 12, 2021
Revised: November 12, 2021
Published: November 23, 2021

https://doi.org/10.1021/acs.langmuir.1c01275
Langmuir 2021, 37, 13976−13984

flow,[23,38] and an analytical theory by Vlahovska and co-workers was also developed to describe the dynamics of a freely suspended lipid bilayer vesicle in a general linear flow.[39] A phase diagram representing the transitions between the three dynamical regimes in shear flow was achieved by varying the viscosity contrast between the vesicle interior and exterior[21] and eventually for a general linear flow.[31] Moreover, an analytical model was further developed to describe transitions between these different dynamical states in a 2D external flow.[40] Zhao and Shaqfeh[24] determined the critical viscosity ratios for the transition from TT to TR to TU regimes using a linear stability analysis based on a spectral boundary integral method, which showed good agreement with experiments. Vesicle dynamics in shear flow has been further studied to include the large deformation of vesicles in the presence of soluble surfactants and role of thermal fluctuation in membrane shape dynamics.[41−48]

In extensional flow, highly deflated vesicles with tubular morphologies ($\nu < 0.6$) transition to symmetric dumbbells above a critical flow strength,[25,27] whereas moderately deflated vesicles with biconcave and spheroidal morphologies ($0.6 < \nu < 0.75$) transition to asymmetric dumbbell shapes in flow.[27,28] A flow-phase diagram for vesicles in extensional flow was recently determined across a wide range of reduced volumes,[29] revealing vesicle morphology in the vicinity of the critical flow strength ($\dot{\epsilon}_{c_1}$) for morphological changes. However, the transient stretching behavior of membrane-bound vesicles above the critical strain rate $\dot{\epsilon}_{c_1}$ has not been systematically characterized. Recent work has focused on the conformational relaxation of highly deformed deflated vesicles ($\nu < 0.75$) following nonlinear deformation into a dumbbell shape in flow.[30] Interestingly, it was found that vesicle relaxation is governed by a double-mode process, with the first stage involving relaxation of the thin lipid nanotube connecting the two spherical bulbs in the dumbbell.[30,49] Vesicle dynamics in a time-dependent extensional flow with a single flow-reversal step was previously reported.[50] Recently, vesicle dynamics in large-amplitude oscillatory extensional flow was studied using a combination of precision flow experiments using the Stokes trap and numerical modeling and simulations.[51] Overall, vesicle stretching in extensional flows generally involves distributed viscous forces across the entire membrane for freely suspended bodies in the absence of external forces. From this view, vesicle deformation in extensional flow is distinct from classical methods used to deform vesicle membranes, e.g. using optical tweezers to pull out thin lipid nanotubes through a localized point force on the membrane[6,7,11,14−16,52−54] or micropipette aspiration.[55,56] Despite recent progress, the transient and steady-state dynamics of freely suspended vesicles in strong flows is not fully understood.

In this work, we directly observe the transient and steady-state stretching dynamics of freely suspended vesicles in extensional flow over a range of equilibrium morphologies including tubular, biconcave, and spheroidal shapes. Our results show that deflated vesicles adopt a steady-state elongated dumbbell shape in flow with highly deformed membrane conformations. We characterize vesicle stretching dynamics over a broad range of vesicle reduced volumes ($0.3 < \nu < 0.95$) by combining fluorescence microscopy with automated flow control, thereby enabling long time observation of vesicles with controlled strain-rate schedules.[57,58] Using this approach, we observe a bevy of nonequilibrium steady-state morphologies for vesicles in strong flow, and we identify a second critical flow strength $\dot{\epsilon}_{c_2}$ above which vesicle stretch diverges in flow. The dependence of the critical flow strength $\dot{\epsilon}_{c_2}$ on vesicle reduced volume is characterized, and this behavior is directly compared to the coil-to-stretch transition for linear polymers and critical deformation of liquid drops in extensional flow. A simple analytical model is developed to describe vesicle membrane stretching dynamics in flow. Comparison with vesicle stretching data shows that the analytical model captures steady-state stretching of vesicles with larger volumes ($\approx \nu > 0.7$); however, it fails to accurately describe the nonlinear stretching of highly deflated vesicles ($\nu < 0.7$). Implications for future development of analytical models are discussed in the context of highly deformed lipid bilayer vesicles.

MATERIALS AND METHODS

Vesicle Preparation. Giant unilamellar vesicles (GUVs) are prepared from a mixture of 1,2-dioleoyl-*sn*-glycero-3-phosphocholine (DOPC) and 0.12 mol % of the fluorescent lipid 1,2-dioleoyl-*sn*-glycero-3-phosphoethanolamine-*N*-(lissamine) rhodamine B sulfonyl (DOPE-Rh) in 100 mM sucrose buffer using an electroformation method, as previously described.[29,59] Briefly, DOPC (25 mg/mL) is mixed with DOPE-Rh dye (0.04 mg/mL) and dissolved in chloroform to prepare a stock lipid solution. Next, 10 μL of this lipid mixture is deposited on a conductive indium tin oxide (ITO) coated glass slide (resistance $\approx$ 35 Ω, 25 × 50 × 1.1 mm, Delta Technologies) and dried under vacuum overnight.[59] An electroformation chamber of volume $\approx$ 2.4 mL was formed using the two ITO slides and a 1.5 mm Teflon spacer and was connected to a function generator (Hewlett-Packard/Agilent 33220 A). The electroformation chamber is filled with 100 mM sucrose solution (Sigma-Aldrich) and an alternating current (AC) electric field of 2 V/mm at 10 Hz is applied for 180 min at room temperature (22 °C). The majority of the vesicles prepared by electroformation method is nearly spherical in shape in the size range of 5−20 μm in radius. The viscosity of the 100 mM sucrose solution (μ = 1.1 mPa·s) is measured using a benchtop viscometer (Brookfield) at 22 °C. To generate deflated vesicles, we used an osmotic deflation method which generates reduced volume vesicles in the range $0.30 < \nu < 0.90$, though the fraction of low reduced volume vesicles ($0.30 < \nu < 0.50$) in the suspension was relatively low. For experiments involving high solvent viscosities (viscosity ratio λ = 0.1), the viscosity of the suspending medium was increased to μ_{out} = 10.4 mPa·s by mixing the 100 mM sucrose solution with glycerol.

Stokes Trap and Automated Flow Control. A Stokes trap[57,58,60] was used in conjunction with an inverted fluorescence microscope (Olympus IX71) on a vibration damping optical table (Thorlabs) (Figure 1). The microscopy setup included a 100 W mercury-arc lamp (USH1002D, Ushio), a 10× magnification air-immersion 0.45 NA objective lens, and a charge-coupled device (CCD) camera (PointGrey GS3-U3-120S6M-C). Standard techniques in soft-lithography[61] are used to fabricate the microfluidic devices, as previously described.[29] Microfluidic devices are mounted on the stage of an inverted microscope, and each of the four inlets of the flow device are connected to a fluidic reservoir (Elveflow XS) containing the buffer solution and the vesicle sample through perfluoroalkoxy (PFA) tubing with 1/16 in. outer diameter and 0.02 in. inner diameter (Figure 1A). Each output line from the fluidic reservoir is also connected to a high precision electronic pressure regulator (Elveflow OB1MKIII), which in turn is connected to a nitrogen cylinder with an output pressure of 30 psi for inducing a pressure driven flow in the microfluidic device.

Single vesicles are trapped in flow near the stagnation point of the microfluidic device using a feedback controlled algorithm[57] (Figure 1B). In brief, freely suspended vesicles are confined in a planar extensional flow using the following approach: (1) images of vesicles in the microfluidic cross-slot device are captured using a CCD camera and vesicle center-of-mass positions are determined using image processing in real-time; (2) a target vesicle is confined in the two-dimensional (2D) flow plane by applying optimal flowrates through the four channels of the microfluidic device using a model-predictive control (MPC) algorithm. This enables precise confinement of vesicles under

https://doi.org/10.1021/acs.langmuir.1c01275
Langmuir 2021, 37, 13976−13984

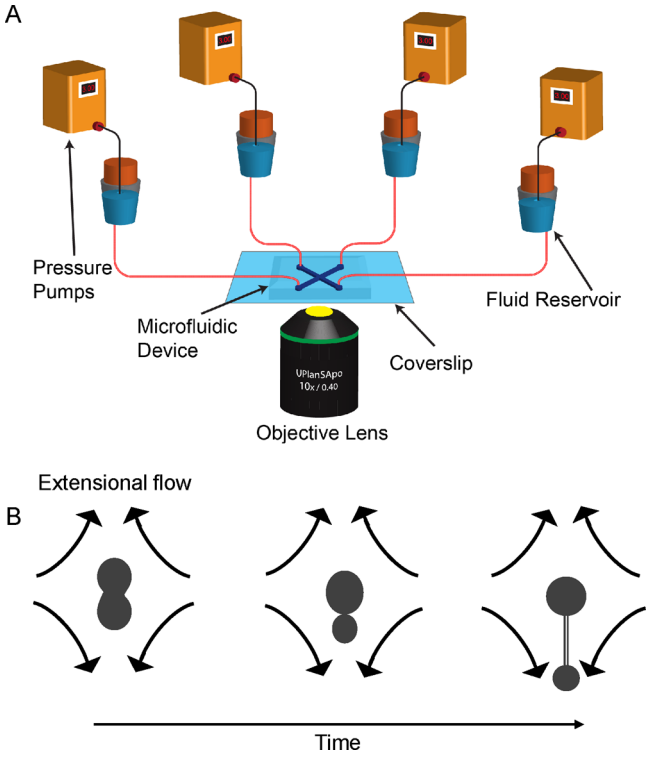

Figure 1. Vesicle stretching dynamics in flow. (a) Experimental setup for the Stokes trap showing the microfluidic device with pressure pumps and fluid reservoirs. (b) Schematic showing the evolution of biconcave vesicle shape under extensional flow due to viscous forces. Initially, the vesicle forms an asymmetric dumbbell shape under flow. At later times, the vesicle continues to elongate with a thin nanotube connecting the two spherical bulbs at the end.

zero flow-rate conditions (using minor flows to counteract Brownian diffusion) or confinement under nonzero net flow conditions. Overall, the Stokes trap allows for the direct observation of vesicle stretching dynamics in precisely controlled flows (e.g., with precise control over the strain rate $\dot{\epsilon}$). To ensure that the flow field is well-characterized during vesicle stretching experiments, we determined the strain rate $\dot{\epsilon}$ using particle tracking velocimetry and bead tracking methods, as previously described.[29]

Relevant Parameters and Dimensionless Groups. Vesicle dynamics are governed by an interplay between membrane bending forces, thermal fluctuations due to excess membrane area, membrane tension under viscous loading, and the viscosities of the interior and exterior fluids. Membrane stretching dynamics are described by three dimensionless groups: (1) capillary number $Ca = \mu_{out}\dot{\epsilon}R^3/\kappa$, which compares the characteristic time scale for bending relaxation to the relevant flow time scale, where μ_{out} is the solvent viscosity, $\dot{\epsilon}$ is the strain rate, R is the equivalent vesicle radius defined in terms of vesicle area A such that $R = \sqrt{A/4\pi}$, and κ is the bending modulus; (2) reduced volume $\nu = 3V\sqrt{4\pi}/A^{3/2}$, which is a measure of vesicle deflation and is defined in terms of a vesicle's volume V, such that $\nu < 1$ corresponds to spheroid, biconcave, or tubular morphologies; and (3) viscosity contrast $\lambda = \mu_{in}/\mu_{out}$, which is the ratio of fluid viscosity between the vesicle interior and exterior. To accurately define Ca, we experimentally determined the average bending modulus of quasi-spherical vesicles at equilibrium to be $\kappa = (22.3 \pm 0.5)k_BT$ using fluctuation spectroscopy, as previously described.[29,62] For all experiments in this work, vesicles are deformed in the bending-dominated regime, such that no area stretching of the membrane occurs.[30]

Nonequilibrium Flow Experiments. To minimize flow-induced shape changes of vesicles prior to studying vesicle dynamics in nonequilibrium flows, GUVs are introduced into the microfluidic device at low flow rates ($\dot{\epsilon} \ll \dot{\epsilon}_{c_1}$). A target vesicle is positioned in the region of interest (ROI) by manually adjusting the pressure difference across the inlets, and the Stokes trap is then used to automatically confine the vesicle near the device center under equilibrium conditions (Figure 1B). The shape of trapped vesicles under zero-flow conditions is recorded and analyzed, and the reduced volume is determined as previously described.[28,29] Next, the fluid strain rate is systematically increased, and vesicle shape dynamics in nonequilibrium flow are directly observed and recorded for postprocessing and analysis (Figure 1B).

RESULTS AND DISCUSSION

Direct Observation of Transient Stretching Dynamics in Flow. We began by studying the stretching dynamics of nearly spherical vesicles ($\nu > 0.9$) following the onset of extensional flow. Here, single vesicles are first trapped near the vicinity of the stagnation point in planar extensional flow in a cross-slot microfluidic device using a Stokes trap (Figure 1).[57,58,60] Vesicles are then observed under zero flow conditions for 10−20 s to determine reduced volume, as previously described.[29,30] At time $t = 0^+$, the vesicle is subjected to a sudden flow onset using a step strain-rate increase. In this way, vesicles are confined in a well-defined extensional flow for long periods of time t or accumulated fluid strain $\epsilon = \dot{\epsilon}t$ while directly observing transient stretching dynamics.[30] Vesicle deformation is quantified by the aspect ratio $A_r = L/L_0 - 1$, where L_0 is the vesicle length at equilibrium. After the onset of flow, quasi-spherical vesicles transition to a steady ellipsoidal shape (Figure S1), consistent with prior work.[13,29] In particular, the vesicle aspect ratio A_r initially increases linearly upon increasing Ca due to unfolding of membrane undulations, and then gradually approaches a maximum value (Figure S2). In all cases, vesicle relax back to the original equilibrium shape after the flow is switched off.

We next studied the transient stretching and relaxation dynamics of vesicles with tubular, biconcave, and spheroidal equilibrium shapes ($0.3 < \nu < 0.75$) (Figure 2). A characteristic series of images highlighting the conformational stretching dynamics of a single vesicle in flow as a function of time ($\nu = 0.64$, $Ca = 23$) is shown in Figure 2A and Movie S1. Remarkably, vesicles are robustly deformed up to ≈10−15× their equilibrium size in flow. For Ca larger than a critical value Ca_{c_1},[28,29] viscous forces overcome bending stresses and drive a morphological transition to a dumbbell shape with a long, thin lipid nanotube connecting the two spherical ends. Interestingly, the radii of two spherical bulbs remain nearly constant during the transient stretching process (Figure 2A). The increase in length of the thin lipid nanotube connecting the end bulbs results from local unfolding of membrane area from the spherical ends of the deformed vesicle. In this way, a shape change which takes the two ends connected by thin tether from a less symmetric to a more symmetric volume distribution contributes to the increase in nanotube length. Transient stretching trajectories are not greatly influenced by membrane thermal fluctuations because the bending modulus is significantly larger than thermal energy ($k_BT/\kappa < 0.04$),[29,30] and vesicles are exposed to strain rates ($Ca > Ca_{c_1}$) much larger than the critical value required for dumbbell formation.

A series of transient stretching trajectories for vesicles with different reduced volumes is shown in Figure 2B. These results include the stretching dynamics of a single vesicle ($\nu = 0.71$) subjected to repeated stretch-relax deformation cycles ($Ca = 39.7, 79.4, 119.1$), which shows that the rate of membrane stretching increases with increasing Ca. In the first cycle ($Ca =$

https://doi.org/10.1021/acs.langmuir.1c01275
Langmuir 2021, 37, 13976−13984

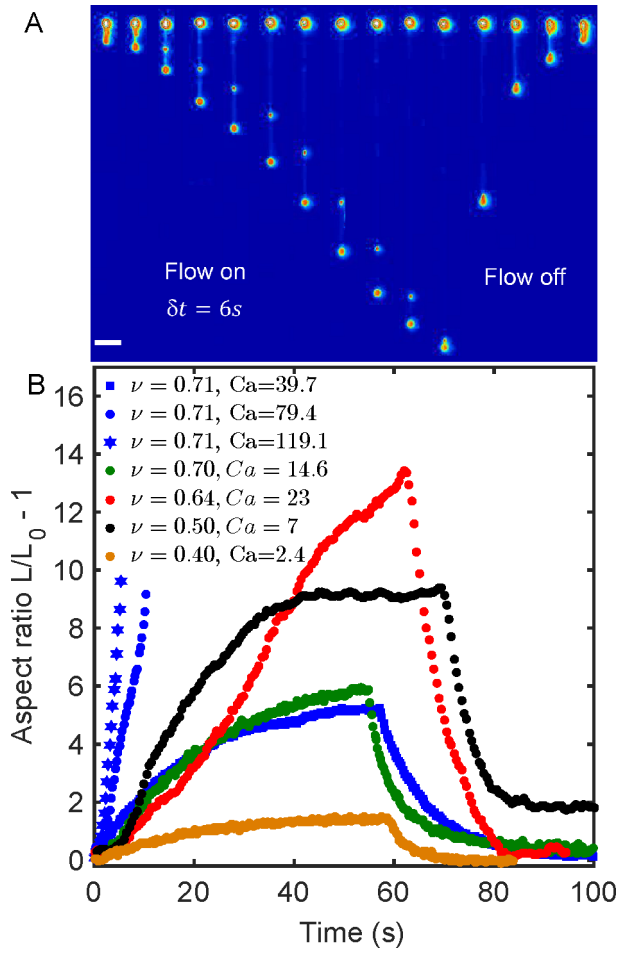

Figure 2. Transient stretching and relaxation dynamics of single vesicles in flow. (a) Snapshots showing temporal evolution of vesicle shape (ν = 0.64) in extensional flow at Ca = 23 showing the formation of an asymmetric dumbbell with a long nanotube tether connecting two spherical end bulbs. The scale bar is 30 μm (SI Movie 1). (b) Transient stretching and relaxation ($L/L_0 - 1$) trajectories of vesicles as a function of time t for a wide range of reduced volume ν and capillary number Ca. Here, the viscosity contrast is λ = 1.

39.7), the vesicle deforms and approaches a steady-state aspect ratio $A_r \approx 5$ after 50−60 s. In the second and third cycles (Ca = 79.4 and 119.1), the vesicle rapidly deforms to $A_r \approx 10$ in only a few seconds, after which the vesicle stretches beyond the field-of-view of the microscope, which generally limits observation of steady-state vesicle deformation to <0.5 mm. Strikingly, these results show that deflated vesicles are highly deformable in flow, such that vesicle membrane integrity is maintained upon repeated deformation in strong flows. In general, this behavior is also observed at a viscosity ratio of λ = 0.1 (Figure S3).

Steady-State Stretching in Flow and Thin Lipid Nanotubes. We next characterized the steady-state deformation of vesicles in flow (Figure 3, Figure S4). Using the Stokes trap, single vesicles are subjected to a series of step increases in strain rate $\dot{\epsilon}$, thereby enabling determination of the steady-state extension for a single vesicle with reduced volume ν as a function of Ca. At each step increment of $\dot{\epsilon}$, the strain rate is held constant for at least 10 s to characterize the steady-state deformation of the vesicle in flow. A characteristic multistep strain-rate experiment for a tubular vesicle (ν = 0.54) is shown in Figure 3A,B. Here, the tubular vesicle is initially trapped at Ca = 0 and $Ca = 2.8 < Ca_{c_1}$, which is smaller than the critical Ca required to induce a transition to a dumbbell conformation[29] (Figure 3A). The flow rate is then increased in a stepwise fashion to Ca = 5.6, after which the vesicle undergoes a morphological change to a symmetric dumbbell with a thin lipid tether connecting two spherical bulbs on the ends of the stretched vesicle. Further stepwise increases of the flow strength to Ca = 8.4 and 11.2 lead to additional deformation of the vesicle in flow (Figure 3A,B). In these experiments, the steady-state value of the aspect ratio A_r is determined as the average of vesicle stretch in the plateau region of the trajectory after transient stretching has ended, with the error bar determined as the standard deviation around the mean.

In prior work, boundary integral simulations were used to study vesicle conformations in extensional flow[27] and accurately captured the dynamics in the vicinity of $Ca \approx Ca_{c_1}$, where vesicle shape transitions from the equilibrium conformation to a dumbbell shape. However, prior numerical simulations and experiments reported no clear steady-state deformation for anisotropic vesicles in strong flow ($Ca > Ca_{c_1}$). In contrast, our

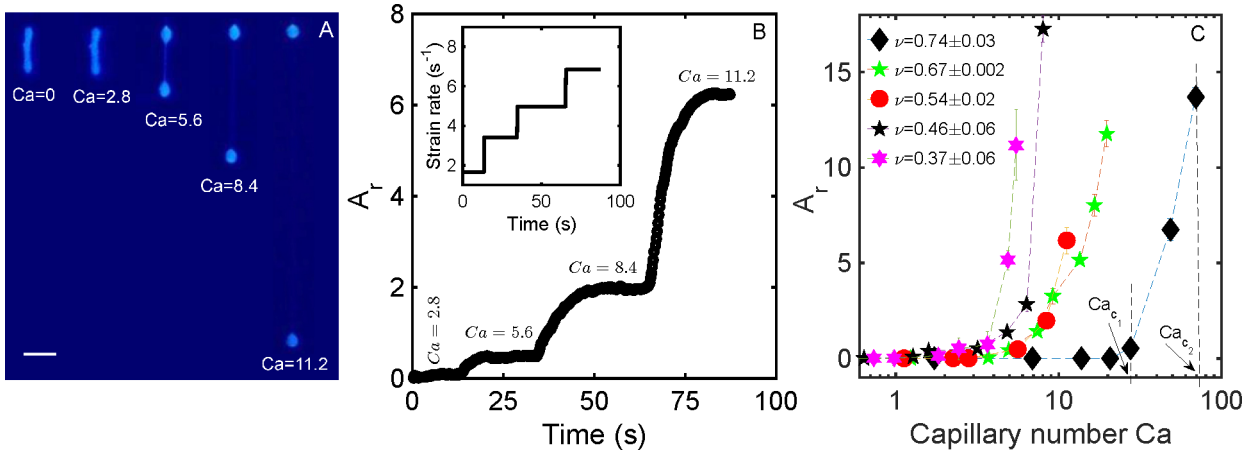

Figure 3. Characterization of steady-state dynamics for different vesicle morphologies. (a) Snapshots of a tubular vesicle (reduced volume 0.54 ± 0.02) showing steady-state dumbbell shapes as a function of Ca. The scale bar is 20 μm. (b) Transient deformation of the tubular vesicle in part a as a function of time upon a stepwise increase in Ca. (inset) Strain rate as a function of time. (c) Steady-state aspect ratio A_r of vesicles as a function of Ca for several reduced volumes ν at a viscosity ratio λ = 1. The aspect ratio for vesicles with $\nu < 0.75$ increases rapidly in a narrow range of Ca beyond a critical value Ca_{c_1} required to induce a symmetric or asymmetric dumbbell. Error bars represent ±1 standard deviation from the mean value.

https://doi.org/10.1021/acs.langmuir.1c01275
Langmuir 2021, 37, 13976−13984

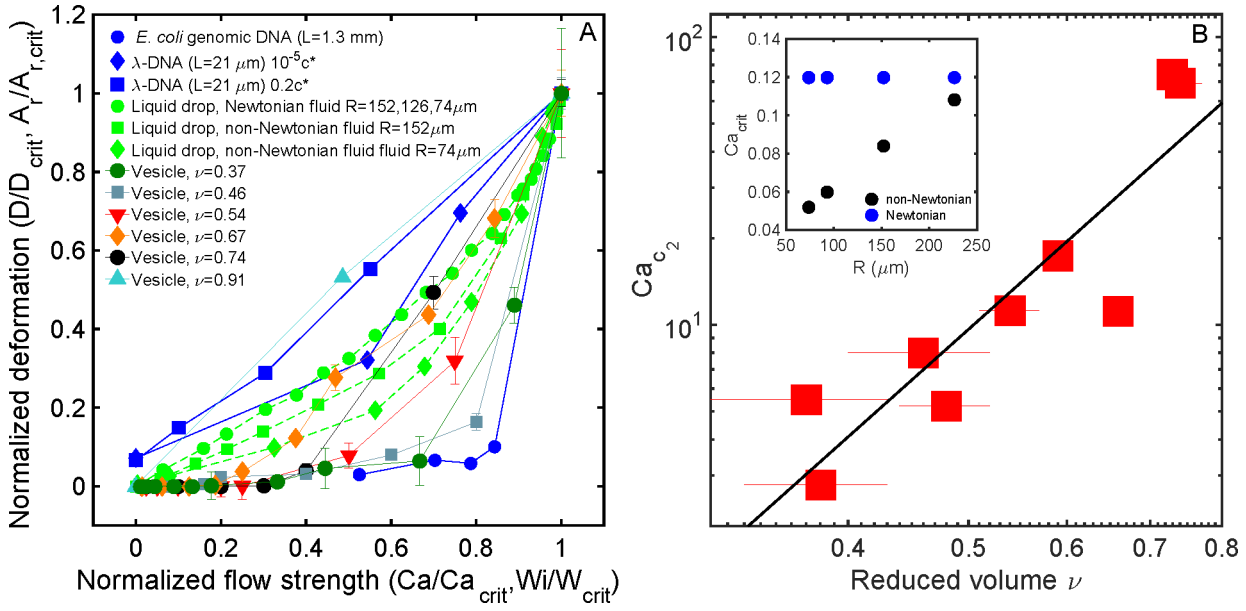

Figure 4. Characterization of critical capillary number Ca_{c_2}. (a) Normalized aspect ratio (A_r), fractional extension, and deformation parameter (D) for vesicles ($\lambda = 1$), polymers, and liquid drops as a function of normalized flow strength (Ca/Ca_{c_2} for vesicles, Ca/Ca_{crit} for drops, Wi/Wi_{crit} for polymers). Error bars represent ±1 standard deviation from the mean value. (b) Log−log plot of Ca_{c_2} as a function of reduced volume ν for viscosity ratio $\lambda = 1$. Red squares represent the experiment, and the black line is a power-law fit of the form $Ca_{c_2} = a\nu^{\beta}$. (inset) Critical capillary number as a function of drop radii for liquid drops suspended in Newtonian and non-Newtonian fluids.

experiments show that vesicles exhibit highly deformed steady-state morphologies over a range of reduced volumes. Broadly speaking, these experiments are uniquely enabled by automated flow control via the Stokes trap, which allows for direct observation of deformed, freely suspended vesicles in well-defined flows for long times.

We systematically investigated the steady-state aspect ratio A_r of moderately deflated ($0.6 < \nu < 0.75$) and highly deflated ($\nu < 0.6$) vesicles over a wide range of Ca at $\lambda = 1$ (Figure 3C). Vesicles with reduced volume $\nu < 0.75$ do not appreciably deform below a critical $Ca < Ca_{c_1}$ as highlighted by vertical dashed line in Figure 3C, which is consistent with prior work.[29] Above a critical value of $Ca > Ca_{c_1}$ required for the morphological transition to a dumbbell shape, vesicles exhibit multiple steady-state conformations upon increasing Ca. The large nonlinear deformation in a narrow range of Ca is consistent with high deformability of low reduced volume vesicles, which arises due to large availability of excess membrane area.[27,30] Above a second critical capillary number Ca_{c_2}, the aspect ratio A_r diverges, highlighted by vertical black dashed line for $\nu = 0.74$ vesicle in Figure 3C. At even higher values of Ca than shown in Figure 3, vesicles presumably adopt additional highly deformed states, though our observations are limited by the finite field-of-view of the microscope. Transient stretching experiments on vesicles with viscosity contrast $\lambda = 0.1$ show a similar overall trend of steady-state deformation as a function of Ca for vesicles with varying reduced volumes (Figure S5).

We further compare our observations for nonlinear vesicle stretching in flow to other soft materials such as single polymer molecules. In extensional flow, linear polymers are known to undergo a conformational transition from the coiled to stretched state at a critical dimensionless flow strength known as the Weissenberg number $Wi_{crit} \approx 0.5$, which roughly corresponds to ≈25% of the Wi at which the polymer stretch reaches a plateau around $Wi \approx 2$.[63] Similarly, in our work, the observed values of Ca_{c_2} correspond to at least 25% of the critical capillary number Ca_{c_3} at which vesicle stretch A_r is predicted to saturate due to the straightening out of all membrane folds in flow (Supporting Information). In particular, we estimate that the maximum length associated with unfolding of all membrane fluctuations lies between 3 and 10 mm depending on vesicle size and reduced volume (Supporting Information). In this way, the observed values of Ca_{c_2} in our experiments lie between 30 and 80% of the predicted critical capillary number Ca_{c_3} at which all of the membrane folds are pulled out in flow. Thus, we take Ca_{c_2} as a critical capillary number for A_r divergence and the corresponding critical deformation as $A_{r,crit}$.

Characterization of Critical Capillary Number Ca_{c_2}. We investigated the nature of the critical capillary number Ca_{c_2} by directly comparing the behavior for vesicles with polymers and liquid drops in extensional flow (Figures 4A,B and S6). Figure 4A plots the normalized aspect ratio $A_r/A_{r,crit}$ as a function of reduced capillary number Ca/Ca_{c_2} for vesicles with different ν. Interestingly, our results show that the transition to critical deformation $A_r \rightarrow A_{r,crit}$ sharpens as the reduced volume is decreased in the limit of $Ca \rightarrow Ca_{c_2}$. This is consistent with the notion that vesicles with small reduced volumes have large excess area and can undergo abrupt deformations in flow. Clearly, a vesicle's reduced volume ν and equilibrium morphology affect the critical stretching dynamics in flow, thereby influencing the nonlinear stretching and critical capillary number Ca_{c_2}.

To directly compare vesicle dynamics with other materials in flow, we plot the normalized deformation parameter (D/D_{crit}) for liquid drops[64,65] and fractional extension for linear polymers in steady extensional flow[66,67] (Figure 4A). In flow, liquid drops

https://doi.org/10.1021/acs.langmuir.1c01275
Langmuir 2021, 37, 13976−13984

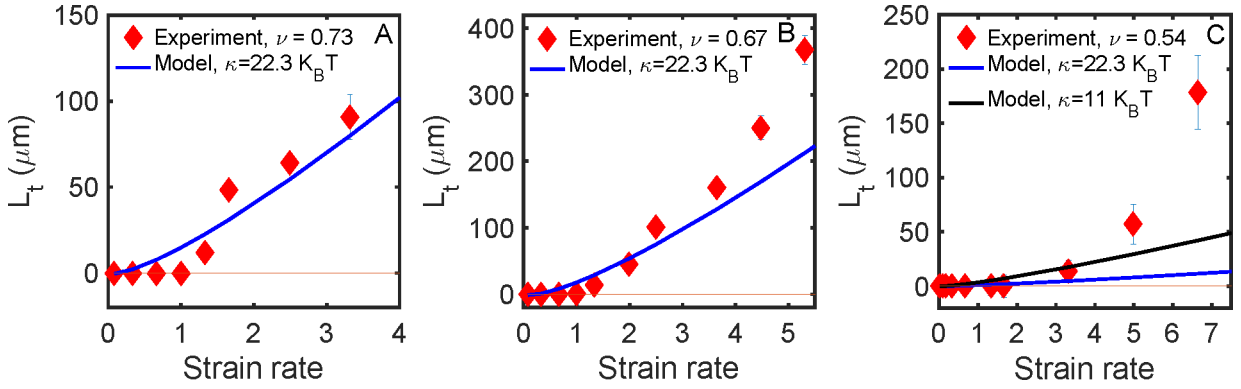

Figure 5. Steady-state stretching of highly deformed vesicles in extensional flow. (A) Experimental data and analytical model prediction of the steady-state nanotube length L_t connecting the two spherical ends of a highly deformed vesicle with $\nu = 0.73$. (B) Experimental data and model prediction of the steady-state nanotube length L_t connecting the two spherical ends of a highly deformed vesicle with $\nu = 0.67$. (C) Experimental data and model prediction of the steady-state nanotube length L_t connecting the two spherical ends of a highly deformed vesicle with $\nu = 0.54$. The orange lines denote zero stretching or $L_t = 0$.

suspended in an immiscible Newtonian fluid are known to exhibit a steady-state deformation (D) up to a critical capillary number, after which drop shape diverges.[64] As the capillary number approaches the critical value ($Ca \rightarrow Ca_{crit}$), the sharpness of transition to critical deformation $D \rightarrow D_{crit}$ for liquid drops in a Newtonian fluid exhibits a universal plot independent of drop size, shown by the green circles in Figure 4A. This universality is lost for drops suspended in non-Newtonian fluids, as the transition to D_{crit} is becomes sharper for liquid droplets with smaller radii due to increasing viscoelastic effects (green squares and diamonds in Figure 4A). Remarkably, these results reveal that the abruptness of transition $A_r \rightarrow A_{r,crit}$ for vesicles is enhanced for smaller reduced volumes due to increasing membrane floppiness; however, the sharpness of transition $D \rightarrow D_{crit}$ for liquid drops is enhanced for smaller radii due to increasing viscoelastic effects in non-Newtonian fluids.

We also compared the critical stretching dynamics of vesicles to linear polymers in extensional flow, where the polymer contour length L and polymer solution concentration c are known to impact the sharpness of the coil-to-stretch transition (CST). As shown in Figure 4A, high molecular weight genomic DNA ($L \approx 1.3$ mm) exhibits a sharper CST as $Wi \rightarrow Wi_{crit}$ compared to λ-DNA ($L \approx 21.1$ μm) in ultradilute solutions ($c \approx 10^{-5}$ c^*).[63,67] In addition, increasing the background polymer concentration from 10^{-5} c^* to ≈ 1 c^* tends to inhibit polymer stretching, such that the CST is far less sharp than ultra dilute solutions as $Wi \rightarrow Wi_{crit}$.[66] From this view, the role of decreasing vesicle reduced volume ν on the steady-state deformation A_r of vesicles (i.e., increased membrane fluctuations and deformability) is analogous to the role of increasing polymer contour length L on the CST transition in extensional flow (i.e., increased polymer extensibility).

We further quantified the critical capillary number Ca_{c_2} as a function of vesicle reduced volume ν (Figure 4B). Interestingly, our results show that Ca_{c_2} follows a power law with ν such that $Ca_{c_2} = a\nu^{\beta}$, where a is a constant and β is the power-law exponent. Our results show that Ca_{c_2} for vesicles follows a power-law dependence on reduced volume, which differs from the behavior of liquid drops, where the critical capillary number is independent of drop size in Newtonian fluids and varies linearly with drop-size in non-Newtonian liquids.

Model for Steady-State Vesicle Deformation. We further sought to develop an analytical model to understand vesicle deformation and membrane elastic properties. For deformed vesicles with symmetric or asymmetric dumbbell shapes, the free energy of a thin nanotube connecting the two spherical bulbs at steady-state (Figure S7) can be written as[6,7,68]

$$E = \frac{1}{2}\frac{\kappa}{r_t^2}2\pi r_t L_t + \sigma 2\pi r_t L_t - fL_t \tag{1}$$

where r_t is the nanotube radius, L_t is the nanotube length, f is the hydrodynamic stretching force, and σ is the membrane tension. Under steady-state conditions, the tube radius and stretching force are estimated by taking the derivative of the free energy such that $\frac{\partial E}{\partial r} = 0$ and $\frac{\partial E}{\partial L} = 0$. In this way, the steady-state tether radius r_t and force f are expressed as $r_t = \sqrt{\kappa/2\sigma}$ and $f = 2\pi\sqrt{2\sigma\kappa}$. Moreover, the increase in tension σ under viscous loading occurs due to an increase in the vesicle area, which can be expressed as[11,68,69]

$$\sigma = \sigma_0 \exp\left(\frac{8\pi\kappa}{k_B T}\frac{A - A_0}{A_0}\right) \tag{2}$$

where σ_0 is the initial membrane tension, k_B is the Boltzmann constant, T is the absolute temperature, A is the observed membrane area at steady-state, and A_0 is the area of initial vesicle conformation (Figures S7 and S8). For a given strain rate $\dot{\epsilon}$, the maximum membrane tension σ_{max} is achieved when the viscous forces on the spherical bulb are balanced by the tether stretching force f. Thus, the force balance is written as $6\pi\mu\dot{\epsilon}R_{\nu_1}^2 = 2\pi\sqrt{2\sigma_{max}\kappa}$, where R_{ν_1} is the radius of upper spherical end (Figure S7). Therefore, the nanotube radius corresponding to the maximum tension is given as $r_{t,min} = \kappa/3\mu\dot{\epsilon}R_{\nu_1}^2$. As previously discussed, the radii of two spherical end bulbs (R_{ν_1} and R_{ν_2}) remain approximately constant during the stretching experiments (Movie S1). Moreover, we assume a simplified vesicle geometry immediately at the onset of conformation changes in flow, as shown in Figures S7 and S8. In this way, the membrane area A at steady-state is given as $A = 4\pi R_{\nu_1}^2 + 4\pi R_{\nu_2}^2 + 2\pi r_t L_t$, and the initial membrane area is $A_0 = 4\pi R_{\nu_1}^2 + 4\pi R_{\nu_2}^2$. Substituting these results into eq 2, the steady-state nanotube

https://doi.org/10.1021/acs.langmuir.1c01275
Langmuir 2021, 37, 13976−13984

length L_t is given as a function of the strain rate $\dot{\epsilon}$ and vesicle parameters:

$$L_t = \frac{3\mu\dot{\epsilon}R_{v_1}^2 k_B T(R_{v_1}^2 + R_{v_2}^2)}{4\pi\kappa^2}\ln\left(\frac{3\mu\dot{\epsilon}R_{v_1}^2}{\sqrt{2\sigma_0\kappa}}\right) \quad (3)$$

In eq 3, κ and σ_0 are membrane properties namely the bending modulus and membrane tension, while the remaining variables are constants related to vesicle geometry and solvent viscosity.

Model Prediction of Steady-State Vesicle Deformation in Flow. We directly compare experimental data for nonlinear vesicle stretching at steady-state to the analytical model given in eq 3 (Figure 5). Here, the steady-state nanotube lengths of several vesicles with different reduced volumes (ν = 0.73, 0.67, 0.54) are plotted as a function of strain rate $\dot{\epsilon}$ with the corresponding analytical model predictions from eq 3. Using fluctuation spectroscopy, we determined the ensemble-averaged bending modulus κ for quasi-spherical vesicles to be $\kappa = 22.3k_BT$ and the average surface tension to be $\sigma = 10^{-7}$ N/m, as described in prior work.[29] In this work, the deflated vesicles are nonspherical at equilibrium, but it is common to assume that membrane properties such as κ for nearly spherical vesicles are relatively constant regardless of global vesicle shape.[29] Overall, the experimental steady-state stretch for vesicles with $\nu = 0.73$ is captured reasonably well by the analytical model (eq 3) (Figure 5A), presumably because the vesicle is moderately deflated and closer to a nearly spherical shape ($\nu \approx 1$).

We further aimed to understand if the experimental steady-state stretching data could be accurately captured by the analytical model for vesicles with smaller reduced volumes ν (e.g., for highly deflated vesicles). However, our results show that the analytical model fails to adequately describe the nonlinear steady stretching dynamics for vesicles with smaller reduced volumes (Figure 5B,C). In particular, the steady-state stretching data for highly deflated vesicles ($\nu = 0.54$) is not well described by the analytical model assuming a constant value of the bending modulus κ. Prior work has shown that individual vesicles with the same membrane composition can exhibit wide variability in bending modulus κ, such that vesicles prepared by identical procedures in different experimental trials can show κ values that vary by a factor of 2.[29,70] We therefore evaluated the analytical model for vesicles with $\nu = 0.54$ using a smaller value of $\kappa = 11k_BT$. However, the analytical model was unable to accurately capture the experimental data, severely under predicting the steady-state nonlinear stretch of vesicles with small reduced volumes. Overall, these observations suggest a few key limitations in the analytical model. First, the analytical model ignores thermal fluctuations of the membrane; however, vesicles with smaller reduced volumes show enhanced thermal fluctuations[25,29,71] (SI Movie 2), which suggests that membrane fluctuations should be considered in the development of more accurate physical models of highly nonlinear membrane stretching for deflated vesicles. In addition, the model does not include contributions from the spontaneous curvature of the membrane. Prior work has shown that such effects may be important for highly deflated vesicles considered in our experiments.[13,68,71] Moreover, area-difference elasticity[72,73] may be important for large tube lengths (>300 μm) considered in our experiments. Overall, our results suggest that deflated vesicles with $\nu < 0.7$ undergo extreme nonlinear deformation within a relatively small of strain rates or Ca. In developing new realistic models for nonlinear membrane stretching, future work should consider membrane undulations, spontaneous curvature, and area-difference elasticity to accurately capture the nonlinear dynamics of deflated vesicles.

CONCLUSIONS

In this work, fluorescence microscopy combined with automated flow control was used to precisely characterize the transient and steady-state nonlinear stretching dynamics of vesicles in flow. Automated flow control offers several advantages for understanding vesicle dynamics in nonequilibrium flows. In particular, the Stokes trap allows for the long time observation of freely suspended vesicles without the need for micropipettes or surface attachment to the membrane interface. In addition, precise control over the flow rate allows for systematic examination of highly deformed steady-state conformations of vesicles over a broad range of reduced volumes ($0.3 < \nu < 0.95$) and capillary numbers Ca. In particular, our work has clearly revealed the nonlinear stretching dynamics in strong flows such that $Ca \gg Ca_{c_1}$.

Using this approach, we characterize the steady-state deformation of vesicles in flow. Our results show that vesicles with reduced volume $\nu < 0.75$ adopt highly elongated dumbbell shapes in strong flows above a critical capillary number Ca_{c_1}, wherein the vesicle steady-state stretch increases nonlinearly with capillary number in flow. Interestingly, our results show that anisotropic vesicles are highly deformable objects, stretching to several millimeters in length in flow, which corresponds to 100−120 times their equilibrium size. The steady-state dynamics of deflated vesicles ($\nu < 0.75$) in flow starkly contrasts with the dynamics of nearly spherical vesicles ($\nu > 0.8$), where the deformed aspect ratio initially increases linearly with capillary number before saturating. Moreover, nearly spherical vesicles adopt a deformed ellipsoid shape in flow, whereas all deflated vesicles adopt a dumbbell shape consisting of two spherical end bulbs connected by a thin tether.

Remarkably, our results reveal a second critical capillary number Ca_{c_2} above which the vesicle aspect ratio diverges for a wide range of reduced volumes ($\nu < 0.75$). Our results show that Ca_{c_2} follows a power-law dependence on reduced volume, which fundamentally differs from the steady-state dynamics of liquid drops in non-Newtonian fluids, where the critical capillary number varies linearly with drop radius, or liquid drops in Newtonian fluids, where the critical capillary number is independent of drop radius. For liquid drops in non-Newtonian fluids, the transition to the critical deformation parameter $D \rightarrow D_{crit}$ becomes less sharp down in the limit $Ca \rightarrow Ca_{crit}$ with increasing drop radius due to a reduction in viscoelastic effects of the suspending fluid. Similarly, in the limit of $Ca \rightarrow Ca_{c_2}$, the sharpness of transition to critical behavior $A_r \rightarrow A_{r,crit}$ decreases upon increasing the reduced volume. Overall, these results suggest that the transition to $A_{r,crit}$ for vesicles with large reduced volumes becomes less abrupt due to a reduction in membrane deformability. Interestingly, polymers also show a less sharp coil-to-stretch transition in extensional flow when the polymer chain extensibility is decreased, e.g. for lower molecular weight polymers. Thus, in the context of critical deformation dynamics in flow, the role of increased reduced volume for vesicles is analogous to the role of decreased molecular weight for polymers and increased radii for liquid drops in non-Newtonian solvents.

Our results provide a direct link between membrane mechanics and vesicle deflation. An analytical model based on

https://doi.org/10.1021/acs.langmuir.1c01275
Langmuir 2021, 37, 13976−13984

only two membrane properties (bending modulus and surface tension) is developed to understand the experimental data, which allows for comparison of the steady-state stretching data to theory for varying amounts of vesicle deflation. Our results show that the analytical model fails to accurately capture the nonlinear vesicle dynamics upon decreasing the reduced volume. These results suggest that additional membrane properties and phenomena such as spontaneous curvature, Gaussian bending modulus, and thermal fluctuations may be important for highly deflated vesicles. Overall, these results provide new insights into the vesicle nonlinear dynamics in strong flows, which is an important step forward in understanding membrane properties for vesicles with different equilibrium morphologies.

■ ASSOCIATED CONTENT

Supporting Information

The Supporting Information is available free of charge at https://pubs.acs.org/doi/10.1021/acs.langmuir.1c01275.

Supplementary figures of the transient dynamics of nearly spherical vesicles (PDF)

Supplementary movies as mentioned in the text (ZIP)

■ AUTHOR INFORMATION

Corresponding Author

Charles M. Schroeder − *Department of Chemical and Biomolecular Engineering, University of Illinois at Urbana−Champaign, Urbana, Illinois 61801, United States; Beckman Institute for Advanced Science and Technology and Department of Materials Science and Engineering, University of Illinois at Urbana−Champaign, Urbana, Illinois 61801, United States;* orcid.org/0000-0001-6023-2274; Email: cms@illinois.edu

Author

Dinesh Kumar − *Department of Chemical and Biomolecular Engineering, University of Illinois at Urbana−Champaign, Urbana, Illinois 61801, United States; Beckman Institute for Advanced Science and Technology, University of Illinois at Urbana−Champaign, Urbana, Illinois 61801, United States;* orcid.org/0000-0002-8971-5912

Complete contact information is available at: https://pubs.acs.org/10.1021/acs.langmuir.1c01275

Notes

The authors declare no competing financial interest.

■ ACKNOWLEDGMENTS

This work was supported by the National Science Foundation under grant no. CBET-1704668. D.K. is grateful for the PPG-MRL Graduate Research Fellowship from the Illinois Materials Research Lab and the Almar T. Widiger Fellowship from the Department of Chemical and Biomolecular Engineering at the University of Illinois at Urbana−Champaign. We thank Channing Richter and Noah Hopkins for help in analyzing the vesicle stretching trajectories.

■ REFERENCES

(1) Noguchi, H.; Gompper, G. Shape transitions of fluid vesicles and red blood cells in capillary flows. *Proc. Natl. Acad. Sci. U. S. A.* **2005**, *102*, 14159−14164.

(2) Park, Y.; Best, C. A.; Badizadegan, K.; Dasari, R. R.; Feld, M. S.; Kuriabova, T.; Henle, M. L.; Levine, A. J.; Popescu, G. Measurement of red blood cell mechanics during morphological changes. *Proc. Natl. Acad. Sci. U. S. A.* **2010**, *107*, 6731−6736.

(3) Dimova, R.; Marques, C. *The Giant Vesicle Book*; CRC Press, 2019.

(4) Lipowsky, R. The conformation of membranes. *Nature* **1991**, *349*, 475.

(5) Discher, B. M.; Won, Y.-Y.; Ege, D. S.; Lee, J. C.; Bates, F. S.; Discher, D. E.; Hammer, D. A. Polymersomes: tough vesicles made from diblock copolymers. *Science* **1999**, *284*, 1143−1146.

(6) Borghi, N.; Rossier, O.; Brochard-Wyart, F. Hydrodynamic extrusion of tubes from giant vesicles. *EPL (Europhysics Letters)* **2003**, *64*, 837.

(7) Rossier, O.; Cuvelier, D.; Borghi, N.; Puech, P.; Derényi, I.; Buguin, A.; Nassoy, P.; Brochard-Wyart, F. Giant vesicles under flows: Extrusion and retraction of tubes. *Langmuir* **2003**, *19*, 575−584.

(8) Riske, K. A.; Dimova, R. Electro-deformation and poration of giant vesicles viewed with high temporal resolution. *Biophys. J.* **2005**, *88*, 1143−1155.

(9) Gracià, R. S.; Bezlyepkina, N.; Knorr, R. L.; Lipowsky, R.; Dimova, R. Effect of cholesterol on the rigidity of saturated and unsaturated membranes: fluctuation and electrodeformation analysis of giant vesicles. *Soft Matter* **2010**, *6*, 1472−1482.

(10) Vlahovska, P. M.; Gracia, R. S.; Aranda-Espinoza, S.; Dimova, R. Electrohydrodynamic model of vesicle deformation in alternating electric fields. *Biophys. J.* **2009**, *96*, 4789−4803.

(11) Dasgupta, R.; Dimova, R. Inward and outward membrane tubes pulled from giant vesicles. *J. Phys. D: Appl. Phys.* **2014**, *47*, 282001.

(12) Wu, S.-H.; Sankhagowit, S.; Biswas, R.; Wu, S.; Povinelli, M. L.; Malmstadt, N. Viscoelastic deformation of lipid bilayer vesicles. *Soft Matter* **2015**, *11*, 7385−7391.

(13) Zhou, H.; Gabilondo, B. B.; Losert, W.; van de Water, W. Stretching and relaxation of vesicles. *Phys. Rev. E* **2011**, *83*, 011905.

(14) Koster, G.; Cacciuto, A.; Derényi, I.; Frenkel, D.; Dogterom, M. Force barriers for membrane tube formation. *Phys. Rev. Lett.* **2005**, *94*, 068101.

(15) Boedec, G.; Jaeger, M.; Leonetti, M. Sedimentation-induced tether on a settling vesicle. *Phys. Rev. E* **2013**, *88*, 010702.

(16) Huang, Z.; Abkarian, M.; Viallat, A. Sedimentation of vesicles: from pear-like shapes to microtether extrusion. *New J. Phys.* **2011**, *13*, 035026.

(17) Vitkova, V.; Mader, M.; Podgorski, T. Deformation of vesicles flowing through capillaries. *Europhys. Lett.* **2004**, *68*, 398−404.

(18) Danker, G.; Vlahovska, P. M.; Misbah, C. Vesicles in Poiseuille flow. *Phys. Rev. Lett.* **2009**, *102*, 148102.

(19) Coupier, G.; Kaoui, B.; Podgorski, T.; Misbah, C. Noninertial lateral migration of vesicles in bounded Poiseuille flow. *Phys. Fluids* **2008**, *20*, 111702.

(20) Kantsler, V.; Steinberg, V. Orientation and dynamics of a vesicle in tank-treading motion in shear flow. *Phys. Rev. Lett.* **2005**, *95*, 258101.

(21) Deschamps, J.; Kantsler, V.; Steinberg, V. Phase diagram of single vesicle dynamical states in shear flow. *Phys. Rev. Lett.* **2009**, *102*, 118105.

(22) Kantsler, V.; Steinberg, V. Transition to tumbling and two regimes of tumbling motion of a vesicle in shear flow. *Phys. Rev. Lett.* **2006**, *96*, 036001.

(23) Misbah, C. Vacillating breathing and tumbling of vesicles under shear flow. *Phys. Rev. Lett.* **2006**, *96*, 028104.

(24) Zhao, H.; Shaqfeh, E. S. The dynamics of a vesicle in simple shear flow. *J. Fluid Mech.* **2011**, *674*, 578−604.

(25) Kantsler, V.; Segre, E.; Steinberg, V. Critical dynamics of vesicle stretching transition in elongational flow. *Phys. Rev. Lett.* **2008**, *101*, 048101.

(26) Zhao, H.; Shaqfeh, E. S. The shape stability of a lipid vesicle in a uniaxial extensional flow. *J. Fluid Mech.* **2013**, *719*, 345−361.

(27) Narsimhan, V.; Spann, A. P.; Shaqfeh, E. S. The mechanism of shape instability for a vesicle in extensional flow. *J. Fluid Mech.* **2014**, *750*, 144−190.

(28) Dahl, J. B.; Narsimhan, V.; Gouveia, B.; Kumar, S.; Shaqfeh, E. S.; Muller, S. J. Experimental observation of the asymmetric instability of intermediate-reduced-volume vesicles in extensional flow. *Soft Matter* **2016**, *12*, 3787−3796.
(29) Kumar, D.; Richter, C. M.; Schroeder, C. M. Conformational dynamics and phase behavior of lipid vesicles in a precisely controlled extensional flow. *Soft Matter* **2020**, *16*, 337−347.
(30) Kumar, D.; Richter, C. M.; Schroeder, C. M. Double-mode relaxation of highly deformed anisotropic vesicles. *Phys. Rev. E: Stat. Phys., Plasmas, Fluids, Relat. Interdiscip. Top.* **2020**, *102*, 010605.
(31) Deschamps, J.; Kantsler, V.; Segre, E.; Steinberg, V. Dynamics of a vesicle in general flow. *Proc. Natl. Acad. Sci. U. S. A.* **2009**, *106*, 11444−11447.
(32) Lin, C.; Narsimhan, V. Shape stability of deflated vesicles in general linear flows. *Physical Review Fluids* **2019**, *4*, 123606.
(33) Coupier, G.; Farutin, A.; Minetti, C.; Podgorski, T.; Misbah, C. Shape diagram of vesicles in Poiseuille flow. *Phys. Rev. Lett.* **2012**, *108*, 178106.
(34) Kaoui, B.; Biros, G.; Misbah, C. Why Do Red Blood Cells Have Asymmetric Shapes Even in a Symmetric Flow? *Phys. Rev. Lett.* **2009**, *103*, 188101.
(35) Fedosov, D. A.; Peltomäki, M.; Gompper, G. Deformation and dynamics of red blood cells in flow through cylindrical microchannels. *Soft Matter* **2014**, *10*, 4258−4267.
(36) Reichel, F.; Mauer, J.; Nawaz, A. A.; Gompper, G.; Guck, J.; Fedosov, D. A. High-throughput microfluidic characterization of erythrocyte shapes and mechanical variability. *Biophys. J.* **2019**, *117*, 14−24.
(37) Keller, S.; Skalak, R. Motion of a tank-treading ellipsoidal particle in a shear flow. *J. Fluid Mech.* **1982**, *120*, 27−47.
(38) Vlahovska, P. M.; Podgorski, T.; Misbah, C. Vesicles and red blood cells in flow: From individual dynamics to rheology. *C. R. Phys.* **2009**, *10*, 775−789.
(39) Vlahovska, P. M.; Gracia, R. S. Dynamics of a viscous vesicle in linear flows. *Phys. Rev. E* **2007**, *75*, 016313.
(40) Lebedev, V.; Turitsyn, K.; Vergeles, S. Dynamics of nearly spherical vesicles in an external flow. *Phys. Rev. Lett.* **2007**, *99*, 218101.
(41) Honerkamp-Smith, A. R.; Woodhouse, F. G.; Kantsler, V.; Goldstein, R. E. Membrane viscosity determined from shear-driven flow in giant vesicles. *Phys. Rev. Lett.* **2013**, *111*, 038103.
(42) Shahidzadeh, N.; Bonn, D.; Aguerre-Chariol, O.; Meunier, J. Large deformations of giant floppy vesicles in shear flow. *Phys. Rev. Lett.* **1998**, *81*, 4268.
(43) Mader, M. A.; Vitkova, V.; Abkarian, M.; Viallat, A.; Podgorski, T. Dynamics of viscous vesicles in shear flow. *Eur. Phys. J. E: Soft Matter Biol. Phys.* **2006**, *19*, 389−397.
(44) Biben, T.; Farutin, A.; Misbah, C. Three-dimensional vesicles under shear flow: Numerical study of dynamics and phase diagram. *Phys. Rev. E* **2011**, *83*, 031921.
(45) Zabusky, N. J.; Segre, E.; Deschamps, J.; Kantsler, V.; Steinberg, V. Dynamics of vesicles in shear and rotational flows: Modal dynamics and phase diagram. *Phys. Fluids* **2011**, *23*, 041905.
(46) Yazdani, A.; Bagchi, P. Three-dimensional numerical simulation of vesicle dynamics using a front-tracking method. *Phys. Rev. E* **2012**, *85*, 056308.
(47) Noguchi, H.; Gompper, G. Dynamics of fluid vesicles in shear flow: Effect of membrane viscosity and thermal fluctuations. *Phys. Rev. E* **2005**, *72*, 011901.
(48) Noguchi, H.; Gompper, G. Fluid vesicles with viscous membranes in shear flow. *Phys. Rev. Lett.* **2004**, *93*, 258102.
(49) Yu, M.; Lira, R. B.; Riske, K. A.; Dimova, R.; Lin, H. Ellipsoidal relaxation of deformed vesicles. *Phys. Rev. Lett.* **2015**, *115*, 128303.
(50) Kantsler, V.; Segre, E.; Steinberg, V. Vesicle dynamics in time-dependent elongation flow: Wrinkling instability. *Phys. Rev. Lett.* **2007**, *99*, 178102.
(51) Lin, C.; Kumar, D.; Richter, C. M.; Wang, S.; Schroeder, C. M.; Narsimhan, V. Vesicle dynamics in large amplitude oscillatory extensional flow. *J. Fluid Mech.* **2021**, *929*, A43.
(52) Sorre, B.; Callan-Jones, A.; Manneville, J.-B.; Nassoy, P.; Joanny, J.-F.; Prost, J.; Goud, B.; Bassereau, P. Curvature-driven lipid sorting needs proximity to a demixing point and is aided by proteins. *Proc. Natl. Acad. Sci. U. S. A.* **2009**, *106*, 5622−5626.
(53) Cuvelier, D.; Chiaruttini, N.; Bassereau, P.; Nassoy, P. Pulling long tubes from firmly adhered vesicles. *EPL (Europhysics Letters)* **2005**, *71*, 1015.
(54) Derényi, I.; Jülicher, F.; Prost, J. Formation and interaction of membrane tubes. *Phys. Rev. Lett.* **2002**, *88*, 238101.
(55) Song, J.; Waugh, R. Bilayer membrane bending stiffness by tether formation from mixed PC-PS lipid vesicles. *J. Biomech. Eng.* **1990**, *112*, 235−240.
(56) Heinrich, V.; Božič, B.; Svetina, S.; Žekš, B. Vesicle deformation by an axial load: from elongated shapes to tethered vesicles. *Biophys. J.* **1999**, *76*, 2056−2071.
(57) Shenoy, A.; Rao, C. V.; Schroeder, C. M. Stokes trap for multiplexed particle manipulation and assembly using fluidics. *Proc. Natl. Acad. Sci. U. S. A.* **2016**, *113*, 3976−3981.
(58) Kumar, D.; Shenoy, A.; Li, S.; Schroeder, C. M. Orientation control and nonlinear trajectory tracking of colloidal particles using microfluidics. *Physical Review Fluids* **2019**, *4*, 114203.
(59) Angelova, M.; Soléau, S.; Méléard, P.; Faucon, F.; Bothorel, P. *Trends in Colloid and Interface Science VI*; Springer, 1992; pp 127−131.
(60) Shenoy, A.; Kumar, D.; Hilgenfeldt, S.; Schroeder, C. M. Flow topology during multiplexed particle manipulation using a Stokes Trap. *Phys. Rev. Appl.* **2019**, *12*, 054010.
(61) Xia, Y.; Whitesides, G. M. Soft lithography. *Annu. Rev. Mater. Sci.* **1998**, *28*, 153−184.
(62) Pécréaux, J.; Döbereiner, H.-G.; Prost, J.; Joanny, J.-F.; Bassereau, P. Refined contour analysis of giant unilamellar vesicles. *Eur. Phys. J. E: Soft Matter Biol. Phys.* **2004**, *13*, 277−290.
(63) Perkins, T. T.; Smith, D. E.; Chu, S. Single polymer dynamics in an elongational flow. *Science* **1997**, *276*, 2016−2021.
(64) Stone, H. A. Dynamics of drop deformation and breakup in viscous fluids. *Annu. Rev. Fluid Mech.* **1994**, *26*, 65−102.
(65) Tretheway, D. C.; Leal, L. G. Deformadtion and relaxation of Newtonian drops in planar extensional flows of a Boger fluid. *J. Non-Newtonian Fluid Mech.* **2001**, *99*, 81−108.
(66) Hsiao, K.-W.; Sasmal, C.; Ravi Prakash, J.; Schroeder, C. M. Direct observation of DNA dynamics in semidilute solutions in extensional flow. *J. Rheol.* **2017**, *61*, 151−167.
(67) Schroeder, C. M.; Babcock, H. P.; Shaqfeh, E. S.; Chu, S. Observation of polymer conformation hysteresis in extensional flow. *Science* **2003**, *301*, 1515−1519.
(68) Dimova, R.; Seifert, U.; Pouligny, B.; Förster, S.; Döbereiner, H.-G. Hyperviscous diblock copolymer vesicles. *Eur. Phys. J. E: Soft Matter Biol. Phys.* **2002**, *7*, 241−250.
(69) Evans, E.; Rawicz, W. Entropy-driven tension and bending elasticity in condensed-fluid membranes. *Phys. Rev. Lett.* **1990**, *64*, 2094.
(70) Nagle, J. F.; Jablin, M. S.; Tristram-Nagle, S.; Akabori, K. What are the true values of the bending modulus of simple lipid bilayers? *Chem. Phys. Lipids* **2015**, *185*, 3−10.
(71) Sanborn, J.; Oglecka, K.; Kraut, R. S.; Parikh, A. N. Transient pearling and vesiculation of membrane tubes under osmotic gradients. *Faraday Discuss.* **2013**, *161*, 167−176.
(72) Seifert, U. Fluid membranes in hydrodynamic flow fields: Formalism and an application to fluctuating quasispherical vesicles in shear flow. *Eur. Phys. J. B* **1999**, *8*, 405−415.
(73) Seifert, U. Configurations of fluid membranes and vesicles. *Adv. Phys.* **1997**, *46*, 13−137.

https://doi.org/10.1021/acs.langmuir.1c01275
Langmuir 2021, 37, 13976−13984